Redox Biology 75 (2024) 103251

Contents lists available at ScienceDirect

Redox Biology

journal homepage: www.elsevier.com/locate/redox

NADPH Alters DUOX1 Calcium Responsiveness

Gregory E. Conner

Department of Cell Biology, University of Miami Miller School of Medicine, 1600 NW 10th Avenue, Miami Fl, 33136, USA

A R T I C L E I N F O

Keywords:
NADPH oxidase
DUOX
Hydrogen peroxide

A B S T R A C T

Hydrogen peroxide is a key element in redox signaling and in setting cellular redox tone. DUOX1 and DUOX2, that directly synthesize hydrogen peroxide, are the most abundant NADPH oxidase transcripts in most epithelia. DUOX1 and DUOX2 hydrogen peroxide synthesis is regulated by intracellular calcium transients and thus cells can respond to signals and initiate responses by increasing cellular hydrogen peroxide synthesis. Nevertheless, many details of their enzymatic regulation are still unexplored. DUOX1 and DUOXA1 were expressed in HEK293T cells and activity was studied in homogenates and membrane fractions. When DUOX1 homogenates or membranes were pre-incubated in NADPH and started with addition of Ca^{2+}, to mimic intracellular activation, progress curves were distinctly different from those pre-incubated in Ca^{2+} and started with NADPH. The Ca^{2+} EC_{50} for DUOX1's initial rate when pre-incubated in Ca^{2+}, was three orders of magnitude lower ($EC_{50} \sim 10^{-6}$ M) than with preincubation in NADPH ($EC_{50} \sim 10^{-3}$ M). In addition, activity was several fold lower with Ca^{2+} start. Identical results were obtained using homogenates and membrane fractions. The data suggested that DUOX1 Ca^{2+} binding in expected physiological signaling conditions only slowly leads to maximal hydrogen peroxide synthesis and that full hydrogen peroxide synthesis activity *in vivo* only can occur when encountering extremely high concentration Ca^{2+} signals. Thus, a complex interplay of intracellular NADPH and Ca^{2+} concentrations regulate DUOX1 over a wide extent and may limit DUOX1 activity to a restricted range and spatial distribution.

1. Introduction

Hydrogen peroxide is a keystone molecule of ROS metabolism (e.g. Ref. [1]). DUOX1 and DUOX2 synthesize H_2O_2 directly [2] and, excluding NOX2 that is highly expressed in phagocytic cells, are the most abundant NADPH oxidase (NOX) transcripts in most epithelial tissues [3]. These enzymes are regulated by Ca^{2+} binding to EF hand motifs [4] and thus can be used by epithelia to produce H_2O_2 when specific needs arise, in contrast to mitochondrial superoxide and H_2O_2 that are byproducts of oxidative phosphorylation. Despite the apparent importance of DUOX1 H_2O_2 synthesis in epithelia, the mechanisms that regulate the enzyme are not well understood.

Recently, DUOX1 cryo-EM structures were reported [5,6]. DUOX1 was complexed with DUOXA1, the known DUOX1 accessory protein required for full activity and stability, and as a dimer of the DUOX1/-DUOXA1 complex. Both structures showed a bound lipid molecule. Purified DUOX1/DUOXA1 specific activity was nearly 10 fold less than membrane bound DUOX1 [5], consistent with the idea that membrane lipid may be required for activity. In both structures, portions of the intracellular domain that contains the EF-hand motifs were not determined, perhaps due to the presence of multiple conformations. Additionally, distances between bound NADPH and FAD appeared too large for efficient electron transfer. Thus, several key features of the structures remain to be elucidated.

Interestingly, epithelial DUOX1 and DUOX2 activities return toward baseline even when intracellular Ca^{2+} is still elevated and this is recapitulated in cell homogenates and membrane preparations [3]. This uncoupling of activity and $[Ca^{2+}]$ was not due to enzyme exhaustion or substrate depletion. The studies presented here examine effects of Ca^{2+} and NADPH on DUOX1 H_2O_2 synthesis in unfractionated cell homogenates and in membrane preparations. These *in vitro* data suggested that the order of NADPH and elevated Ca^{2+} exposure favored different Ca^{2+} sensitivities and levels of activity. Preincubation with NADPH in low $[Ca^{2+}]$ expected in cytosol, resulted in a low activity DUOX1, that could be slowly increased by increasing Ca^{2+}; however, very high concentrations of Ca^{2+} were required for full activation of DUOX1. The data offer a possible an explanation for decreased DUOX1 activity in the continuous elevated intracellular $[Ca^{2+}]$ and suggest a mechanism that could restrict DUOX1 activity to a narrower range *in vivo*.

Abbreviations: HRP, horseradish peroxidase; HB, homogenization buffer; PM, plasma membrane; SOD, superoxide dismutase.

E-mail address: gconner@miami.edu.

https://doi.org/10.1016/j.redox.2024.103251
Received 23 May 2024; Received in revised form 14 June 2024; Accepted 20 June 2024
Available online 20 June 2024

2. Methods

Cells: HEK293T cells expressing human DUOX1/DUOXA1α were grown and maintained as previously described at 37° in 5 % CO_2 in DMEM, supplemented with 10 % FCS [3,7]. Both DUOX1/DUOXA1 and empty vector cell lines were constructed using pCDH lentiviral vectors ([7] and Supplemental methods). DUOX1/DUOXA1 transduced cells showed large increases in H_2O_2 synthesis after transduction [3,7], while untransduced cells and cells transduced with empty vector showed low levels of H_2O_2 synthesis. The H_2O_2 synthesis rate in DUOX1 expressing cells was 80 fold higher than that of cells transduced with empty vector (supplementary figure in Ref. [7]).

Preparation of extracts: Homogenization was described previously [3]. All steps were carried out at 4°. Briefly, confluent cultures were washed with PBS with 1 mM EDTA pH 7.4 and then with homogenization buffer (HB) (25 mM K acetate, 10 mM HEPES, pH 7.6, 1 mM MgCl2, 10 μM leupeptin, benzamidine, aprotinin, pepstatin, PMSF, 1 mM β-glycerophosphate and Na pyrophosphate). Cells were scraped into homogenization buffer, incubated on ice for 15 min, collected by 600×*g* centrifugation for 5 min, and broken using a Dounce homogenizer while monitoring by phase contrast microscopy. Sucrose was added to 0.25 M and protein concentration determined using Pierce™ BCA Protein Assay. Homogenates were snap frozen in liquid N_2 and stored at −80°.

Membrane preparations: Homogenates were centrifuged at 1000×*g* for 5min, followed by centrifugation of the supernatant at 7000×*g*, for 10 min and resuspension of the 7000×*g* pellet in 0.25 M sucrose in HB. A plasma membrane (PM) enriched fraction was prepared by diluting the resuspended 7000×*g* pellet with 2.5 M sucrose to give 1.4 M final, overlaying with 0.25 M sucrose in HB and centrifuging at 150,000×*g* for 1 h. The PM-enriched fraction that floated to the 0.25 M/1.4 M interface, was collected, diluted with 2 vol of ice cold water and 1 volume of 0.25 M sucrose in HB, and centrifuged for 30 min at 8000×*g*. The 7000×*g* supernatant was used to prepare a microsomal fraction by centrifugation at 100,000×*g* for 1 h. Pellets were resuspended in 0.25 M sucrose HB, snap frozen in liquid N_2 and stored at −80°. Protein was determined by BCA assay,.

Hydrogen peroxide assays: Enzyme activity in homogenates and membranes was measured via Amplex Red-horseradish peroxidase (HRP) assay as previously described [3]. Briefly, 5 μl of homogenates or membranes (5–20 μg) were added into pre-warmed, black, 96 well plates and 95 μl of reaction buffer (25 mM HEPES pH 7.2, 1 μM FAD, 1.5 mM $MgCl_2$, 0.1 μM thapsigargin, 30 μM 10-Acetyl-3,7-dihydroxyphenoxazine (Cayman Chemicals, Amplex red), 0.15 U/ml HRP) were added. Reaction buffer also contained either NADPH or buffered Ca^{2+}. Plates were placed into a Biotek Synergy H1 reader at 27° for 5–10 min to equilibrate before starting reactions with 10 μl of either NADPH or Ca^{2+} containing solutions. Assay temperature equilibration times in the Synergy H1 were predetermined using sulforhodamine fluorescence (520 nm ex/600 nm em) [8,9]. Resorufin fluorescence (530ex/590em) was measured and initial rates estimated using the first three data points typically 240 s. Although the assays were nonlinear in this time frame, using the first three points reduced the variation encountered when calculating with only one point that was confounded by slight fluctuation of times from addition and mixing of the solution to the first recorded point obtained in the plate reader.

Amplex red undergoes photo-oxidation and can be oxidized by HRP and NADPH possibly confounding measurement of H_2O_2 (for review see Ref. [10]). Protection from continuous light exposure [11], inclusion of SOD and keeping NADPH concentrations below 50 μM serve to limit artifactual oxidation [12,13]. Cell homogenates contain endogenous superoxide dismutase (SOD) and assays were sampled at intervals by flash lamp that limited light exposure. In addition, all assays contained, in parallel, control homogenates or membrane fractions from HEK293T cells transduced with empty vectors [3,7] to normalize DUOX1 values. Thus, any background oxidation of Amplex red, including minor amounts of H_2O_2 synthesized by endogenous NADPH oxidases or derived from mitochondria or other sources were subtracted from signals obtained with DUOX1-DUOXA1 expressing cells. All experiments included H_2O_2 (0–500 nM) standard curves in the used reaction buffers. H_2O_2 concentrations were confirmed by absorption at 240 nm using 43.6 $M^{-1}cm^{-1}$ extinction coefficient. Previously, homovanillic acid assay and post hoc Amplex red assays gave identical results to this real time Amplex red assay [3] when using whole cell homogenates.

Membrane fractions were depleted of endogenous SOD, that is needed to suppress HRP-mediated redox cycling of NADPH and Amplex Red [12], and catalase that consumes H_2O_2 is concentrated in microsomes. For this reason, SOD (250 U/ml) and NaN_3 (200 μM) were added to assays of membrane fractions. Addition of SOD to membrane fraction assays very slightly decreased measured H_2O_2 synthesis most likely by blocking HRP/NADPH cycling that leads to Amplex red oxidation [12]. In assays with high concentrations of NADPH (≥100 μM), SOD was insufficient to control HRP-mediated NADPH and Amplex Red cycling and in those conditions, a post-hoc assay was used (Supplemental methods).

Calcium solutions were buffered with EGTA, NTA and HEDTA as described previously [3]. NTA and HEDTA concentrations ranged from 0.1 to 3 mM and EGTA concentrations ranged from 0.3 to 3.3 mM. Calculations to determine Ca^{2+}, Mg^{2+} and chelator concentrations were made with WEBMAXC software program [14] (https://somapp.ucdmc.ucdavis.edu/pharmacology/bers/maxchelator/webmaxc/webmaxcS.htm) and checked by calcium electrode.

NADPH stock solution concentrations were confirmed by 340 nm absorbance (extinction coefficient, 6220 M^{-1} cm^{-1}). NADPH consumption (Supplemental Figs. 1A and B) was determined by fluorescence (340 nm ex/460 nm em). Although other molecules such as nucleotides, fluoresce at these wavelength, addition of 50 μM NADPH into assays increased fluorescence values 20 fold over reaction values before addition decreasing the likelihood of confounding signals from other molecules.

Curve fitting and statistics are described in figure legends and in Supplemental methods.

3. Results and discussion

Published *in vitro* assays of DUOX1 activity have typically been initiated by addition of NADPH to enzyme preparations previously incubated in Ca^{2+} (e.g. Refs. [3,15,16]). Here, in a similar fashion, homogenates of DUOX1/DUOXA1 expressing HEK cells were preincubated in increasing [Ca^{2+}] for 5–10 min and H_2O_2 synthesis was followed after addition of 50 μM NADPH (Fig. 1A). Initial rates were calculated after subtraction of values obtained with empty vector controls and used to calculate an EC_{50} (shown in Fig. 1C). To more closely mimic *in vivo* conditions where NADPH is normally present before Ca^{2+} elevation, assays were performed by incubating homogenates in 50 μM NADPH and then activating DUOX1 by addition of increasing [Ca^{2+}] (Fig. 1B). The EC_{50}, after first exposing to NADPH followed by Ca^{2+} activation was 3 orders of magnitude higher (Fig. 1C; red squares, 0.3 mM, CI95 = 0.1–0.5 mM) than exposure to Ca^{2+} before NADPH (Fig. 1C; black circles,1.6 μM, CI95 = 0.9–2.9 μM). Additionally, stimulated maximum activity was reduced >2 fold in homogenates preincubated with NADPH and started by Ca^{2+} addition. The reduction in activity was not due to consumption of NADPH during the experiment as the [NADPH] was minimally reduced (measured concurrently by 340 nm ex/460 nm em fluorescence, Supplemental Figs. 1A and 1B)). In both cases, Ca^{2+} behaved as an essential activator with no activity apparent in nominally zero [Ca^{2+}]. Repeated experiments (Fig. 1D) confirmed that the EC_{50} derived from the two types of assays differed by ~1000 fold (Fig. 1D, 2.3 ± 1.3 μM (SD) n = 16 vs. 1.9 ± 1.2 mM (SD) n = 5, $p < 0.0001$).

Since [Ca^{2+}] in the cytosol is not zero but is estimated to be below 100 nM (e.g. Ref. [17]), NADPH was added to homogenates previously adjusted to 100 nM Ca^{2+}, followed by starting reactions with increasing [Ca^{2+}]. The EC_{50} remained very high (Fig. 1C; blue triangles, 0.96 mM,

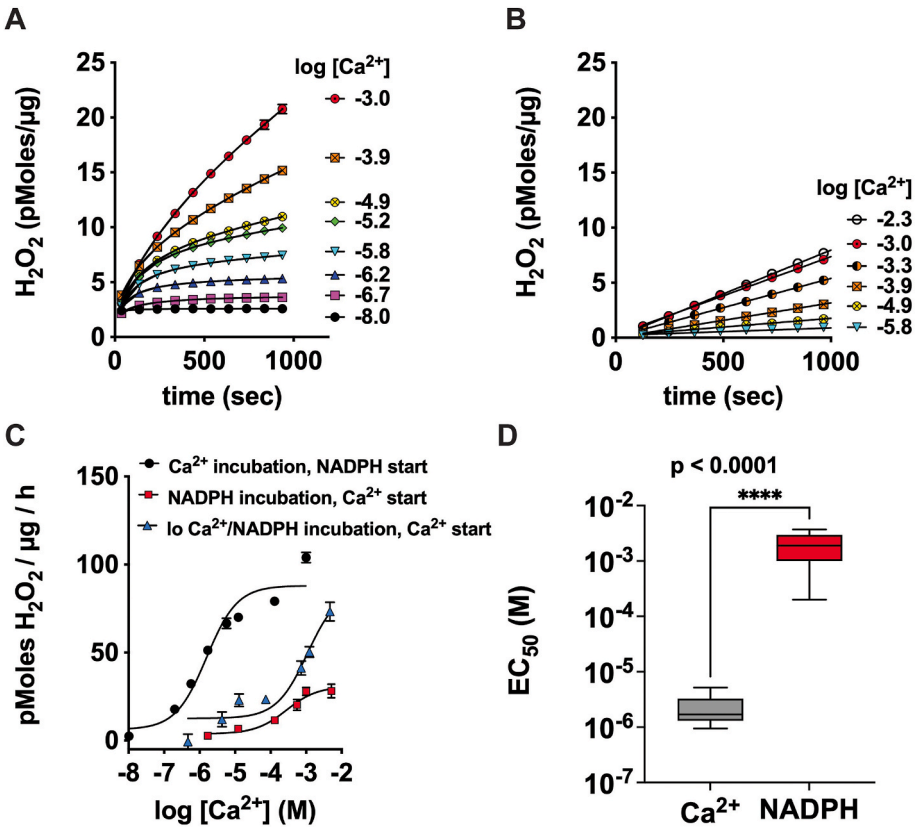

Fig. 1. Preincubation of homogenates in NADPH alters DUOX1 Ca^{2+} sensitivity. *Panel A*, Homogenates were preincubated with increasing [Ca^{2+}] and reactions were started by addition of 50 µM NADPH. Resorufin fluorescence was measured at timed intervals and H_2O_2 calculated from parallel standard curves. Progress curves were fit to a double exponential (equation 3 in Ref. [35], *viz.* Supplemental methods) using Graphpad Prism 9. *Panel B*, homogenates were preincubated with 50 µM NADPH and reactions were started by addition of increasing [Ca^{2+}]. Resorufin fluorescence was measured at timed intervals and H_2O_2 calculated as in panel A. *Panel C*, EC50's for Ca^{2+} were obtained by fitting initial rates of reactions to a 3-parameter dose response curve using Graphpad Prism 9 for reactions shown in panel A preincubated in various [Ca^{2+}] and started with NADPH (1.6 µM, CI95 = 0.9–2.9 µM, black circles in panel C); using reactions shown in panel B preincubated in NADPH and started with various [Ca^{2+}] (0.3 mM, CI95 = 0.4–2.6 mM, red squares panel C); and using reactions preincubated with sequential addition of 100 nM Ca^{2+} followed by NADPH and finally starting reactions with addition of various higher [Ca^{2+}] (progress curves not shown) (0.96 mM, CI95 = 0.34–2.2 mM, blue triangles panel C). *Panels A - C* are mean values of triplicate assays ± S.D. from a single experiment. Some error bars are within the symbols. *Panel D*, mean EC_{50} values from repeated experiments, as described in panel A (Ca^{2+} preincubation) and B (NADPH preincubation), were respectively, 2.3 ± 1.3 µM (SD), n = 16 and 1.9 ± 1.2 mM (SD), n = 5, $p < 0.0001$, Mann-Whitney test.

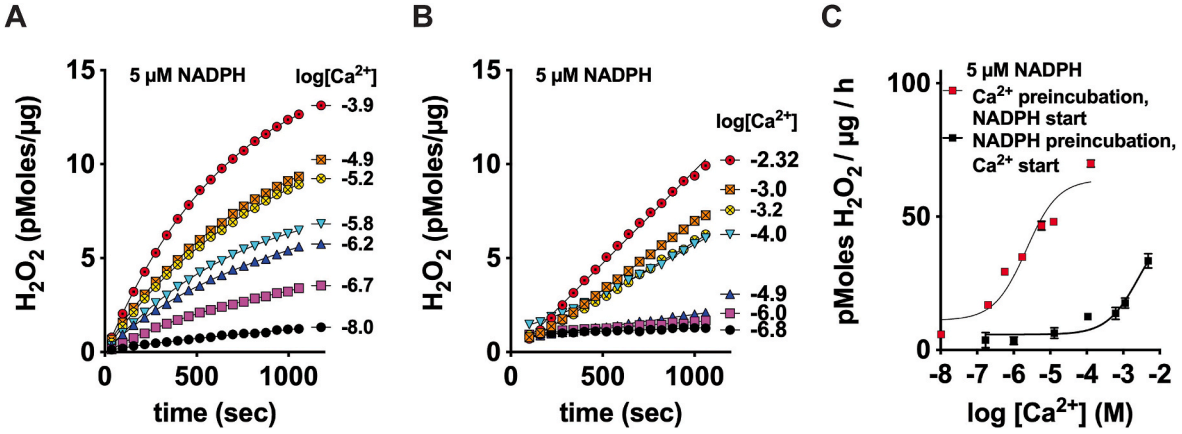

Fig. 2. Preincubation of PM-enriched fractions in NADPH alters DUOX1 Ca^{2+} sensitivity. *Panel A*, PM-enriched fractions were preincubated with increasing [Ca^{2+}] and reactions were started by addition of 5 µM NADPH. Resorufin fluorescence was measured at timed intervals and H_2O_2 calculated from parallel standard curves. Progress curves were fit to a double exponential (equation 3 in Ref. [35], *viz.* Supplemental methods) using GraphPad Prism 9. *Panel B*, Homogenates were pre-incubated with 5 µM NADPH and reactions were started by addition of increasing [Ca^{2+}]. Resorufin fluorescence was measured at timed intervals and H_2O_2 calculated as in panel A. *Panel C*, The EC50 was calculated from Ca^{2+} dose response curves: using reactions shown in panel A preincubated in various [Ca^{2+}] and started with NADPH (2.2 µM, CI95 = 0.9–5.6 µM, red circles in panel C) and using reactions shown in panel B preincubated in NADPH and started with various [Ca^{2+}] (2.5 mM, CI95 = 1.2–8.2 mM, black squares panel C). EC_{50}'s for Ca^{2+} were obtained by fitting initial rates of reactions to a 3-parameter dose response curve using GraphPad Prism 9. *Panels A-C* are mean values of triplicates ± S.D. from a single experiment. Some error bars are within the symbols.

CI95 % = 0.34–2.2 mM). These data suggested that full activation of DUOX1 H_2O_2 synthesis in *vivo*-like conditions (i.e. in the presence of NADPH and basal [Ca^{2+}]) requires very high local intracellular [Ca^{2+}].

It was possible that preincubation of homogenates with NADPH altered thioredoxin and glutathione redox cycles that in turn impacted measurement of H_2O_2 synthesis. Additionally, although cytosolic NADPH has been variously reported to be 10–50 μM [18–20], it was possible that 50 μM NADPH is above the physiological concentration since a recent report using a biosensor protein estimated [NADPH] at 3 μM [21]. To address both possible confounders, a PM-enriched membrane fraction was used with either NADPH or Ca^{2+} preincubation using 5 μM NADPH in both cases. Assays of the PM fraction showed similar ~1000 fold increase in EC_{50} when exposed first to NADPH followed by Ca^{2+} to start synthesis (Fig. 2). Since the PM-enriched fraction is expected to be depleted of both thioredoxin and glutathione and their redox cycling enzymes, these data suggested that neither NADPH-induced perturbation of the redox tone nor excessively high NADPH were plausible explanations for the differences in EC_{50}.

It was possible HRP-mediated formation of an inhibitory $NADP^{\bullet+}$ radical [12] could be responsible for shifting EC_{50}. To address that possibility, the PM-enriched fraction, preincubated with NADPH and started with Ca^{2+}, was also assayed by a post-hoc procedure in which HRP or Amplex red is not present in the reactions. Instead, timed samples are taken for H_2O_2 assay by stopping the reaction with HCl to allow NADPH decomposition (see Supplementary methods). Hydrogen peroxide was then assayed by HRP and Amplex Red. Similar results were obtained ruling out HRP-mediated artifacts (Supplementary Fig. 1C). These data were recapitulated using the microsomal fraction that possibly represented nascent DUOX1 that had not reached the cell surface (Supplementary Fig. 2).

Global intracellular [Ca^{2+}] signals do not reach such high levels as those used in the assay, and additionally, persistent high [Ca^{2+}] is cytotoxic; however, microdomains of locally high intracellular [Ca^{2+}] concentrations have been measured. Although methods are not readily available to quantify microdomain [Ca^{2+}] in the molecular scale space surrounding Ca^{2+} channel pores, multiple authors have computationally modeled expected [Ca^{2+}] near channel pores and propose that [Ca^{2+}] can be expected to reach high μM (e.g. Refs. [22,23]). These studies have shown that very near the channel opening, concentration is determined by flux and diffusion with little effect coming from pumps and buffers that limit concentrations at greater distances. In this regard, others show in several cell lines that DUOX1 co-immunoprecipitates with the large conductance Ca^{2+} channel, IP3R1 [24], that exists both in the ER and in the plasma membrane [25] suggesting that DUOX1 could possibly encounter a high [Ca^{2+}] microdomain or nanodomain during IP3R release of Ca^{2+} from intracellular stores or by entry at the plasma membrane [25]. Although an EC_{50} near 1 mM is not expected for Ca^{2+} stimulation of EF hand domain proteins, others have reported EF hand Ca^{2+} affinities in the mM range (e.g. Refs. [26–28]).

The extracellular peroxidase homology domain of mouse DUOX1 contains a cation binding site believed to be occupied by Ca^{2+} [6]. This site is conserved in human DUOX1 and corresponds to the Ca^{2+} binding site in lactoperoxidase. Although possible, it seems unlikely that Ca^{2+} binding to this site that is exposed to high extracellular [Ca^{2+}] would alter enzyme activity initiated on the other face of the membrane.

Progress curves of assays preincubated in Ca^{2+} and started with NADPH showed an initial burst followed by a slower linear rate of synthesis (Fig. 3). This biphasic progress curve was highly similar, but not identical, to those observed with slow transient kinetics (e.g. Refs. [29,30]). In contrast, progress curves of assays preincubated in NADPH and started with Ca^{2+} addition showed a very slowly increasing rate (Fig. 3B). Similar nonlinear progress curves were observed with PM. Shape dependence of progress curves on starting conditions was described by Morrison with reference to slow binding inhibitors [29] and by Waley regarding substrate inhibition [31]. This change in curve shapes dependent on initial conditions ruled out a number of trivial explanations for nonlinear progress curves. These include artifacts of instrument response, temperature equilibration or slow incomplete mixing (both also ruled out experimentally), and slow or incomplete responses of the AR/HRP detection system.

Possible contamination of substrate with an inhibitor, that can be responsible for nonlinear progress curves, was ruled out by assays with increasing amounts of product ($NADP^+$), nicotinamide or NADH, known to be low concentration contaminants of NADPH (Supplemental Figs. 1D and 1E). Increasing $NADP^+$ to 20 μM did not lower the initial rate compared to controls ruling out that product accumulation could explain the biphasic progress curves (Supplemental Fig. 1D).

Other possible mechanisms that may account for the observed progress curves are: slow inhibition by substrate, slow structural changes required for activation such as tertiary structural changes, possible interaction of DUOX1 with a bound [32] and slowly dissociating inhibitor, a shift between the DUOX1/DUOXA1 dimer and the tetrameter observed in cryo-EM structures [5,6] or activation of the protein by post-translational modification.

To assess whether substrate inhibition could account for the nonlinear progress curves, assays were conducted with increasing

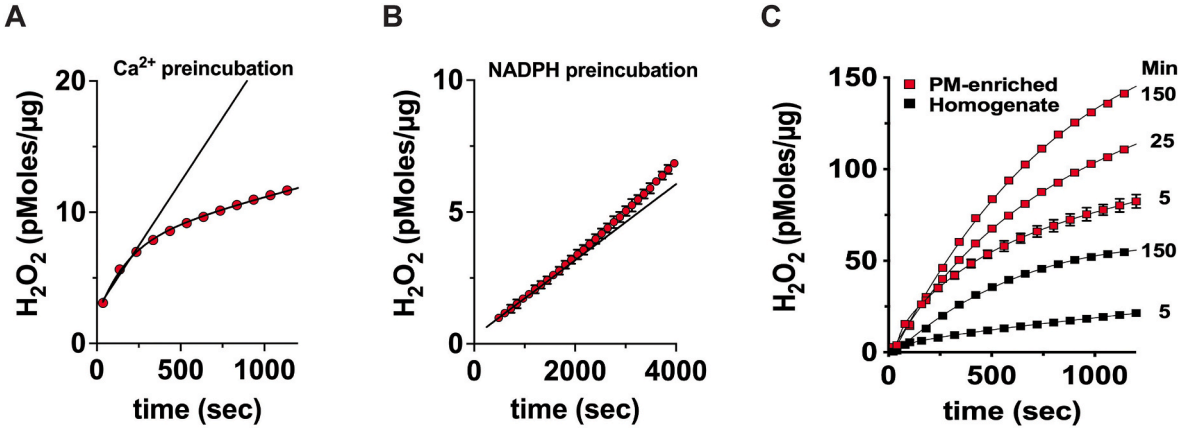

Fig. 3. DUOX1 progress curves are nonlinear. *Panel A*, Homogenates were preincubated in 12 μM Ca^{2+} and reactions were started with 50 μM NADPH, and in *Panel B*, homogenates were preincubated in 50 μM NADPH and started by addition of Ca^{2+} to 12 μM. Lines represent the slope over the first three data points. Preincubation in Ca^{2+} showed an initial burst of activity followed by a slower rate. Conversely, preincubation with NADPH showed a lower initial rate that slowly increased with longer reaction times. *Panel C*. Homogenates (black squares) or PM-enriched fractions (red squares) were preincubated in 12 μM Ca^{2+} for 5, 25 or 150 min as indicated in the graph before starting with 50 μM NADPH addition. Preincubation in Ca^{2+} increased the activity. Plotted values are means of triplicate assays. Some error bars are within the symbols.

[NADPH]. Initial studies suggested that substrate inhibition might account for the observations; however, at starting NADPH concentrations ≥100 μM, HRP-mediated NADPH redox-cycling [12] confounded assays by reducing the [NADPH] as measured by fluorescence (340ex, 460em). To avoid NADPH depletion during preincubation with HRP and Amplex Red, and to avoid HRP-mediated generation of $NADP^{\bullet+}$ radical [12], post-hoc assays of homogenates and membrane reactions were carried out in the absence of HRP and Amplex Red. Reactions were stopped with HCl to decompose NADPH, neutralized and then assayed by HRP and Amplex red (See Supplemental methods). These post-hoc assays using preincubation with increasing concentrations of NADPH and a Ca^{2+} start did not show substrate inhibition (Supplemental Fig. 3A).

To explore slow structural changes, slow Ca^{2+}-mediated dissociation of bound inhibitors or post-translational modifications as potential mechanisms to explain the biphasic progress curves, homogenates and membranes were preincubated in Ca^{2+} for increasing time periods followed by NADPH initiation. These data showed that increased exposure time in Ca^{2+} shifted the progress curve towards the initial burst and away from the later lower activity (Fig. 3C) consistent with the idea that one of the above mentioned mechanisms could explain nonlinear progress curves. Slow Ca^{2+} mediated structural transitions might explain the low resolution of the DUOX1 intracellular domain in cryo-EM studies [5,6]. Similar shifts in DUOX2 activity were also seen after increasing incubation times in Ca^{2+} (Supplemental Fig. 1F). It was possible that Ca^{2+} induced changes were a result of calpain activation and cleavage. Leupeptin (10 μM) was included in the homogenization buffer and inhibits both μ and *m*-calpain with a Ki ≤ 1.5 [33]. In addition, no calpain cleavage sites were found in DUOX1 and DUOXA1 using the deep machine learning program DeepCalpain [34] on the lowest detection threshold. Thus, it was unlikely that calpain cleavage was responsible for the observed Ca^{2+} induced changes. No qualitative or quantitative changes of progress curves were observed after longer preincubation in NADPH in the absence of Ca^{2+}, followed by addition of Ca^{2+} to start the reactions, although these studies were confounded by slow consumption of NADPH during longer preincubations.

Others have shown that PKA phosphorylation increases DUOX1 activity [4] and Ca^{2+} activates adenylyl cyclase. To test whether phosphorylation could alter activity during the reactions or be responsible for nonlinear progress curves, 5 mM ATP was added to homogenate reaction mixes preincubated in Ca^{2+} before starting with NADPH. Corrections to added Ca^{2+} and Mg^{2+} were made to account for ATP chelation. No changes in progress curve shape, maximal activity or EC_{50} were observed (Supplemental Figs. 3B and C). Nonlinear progress curves were observed with the PM-enriched fraction that should not contain PKA consistent with the idea that phosphorylation is not responsible for the differences in EC_{50}. The published *in* vivo increase in DUOX1 activity due to PKA-dependent phosphorylation occurs over several hours [4], and although no changes in cell surface expression were noted, these intact cell assays also measured intracellular H_2O_2 synthesis. Thus, the data here might suggest that the previously published PKA-mediated increased DUOX1 activity could be due to indirect effects, perhaps increased stability or decreased turnover.

Although speculative, NADPH may significantly slow the expected Ca^{2+} dependent DUOX1 conformational change needed for enzyme activation either through binding to DUOX1 or through other NADPH dependent changes in DUOX1 structure. For example modification of cysteines, either in DUOX1 or other associated proteins, could be affected. A possible instance might be DUOX1 Cys1520 SG that is near (4.4 Å) NADPH C4N (PDB IDs: 7D3E and 7D3F). It is also possible that the Ca^{2+} affinities of the two EF hand domains are very different and structural rearrangement after NADPH binding differentially changes the sensitivity to Ca^{2+} binding by one or both of these. A full understanding of how NADPH binding alters Ca^{2+} sensitivity will require a clearer picture of the DUXO1/DUOXA1 intracellular domain structure in conditions that resemble those encountered *in vivo*.

4. Conclusion

The data presented here showed that Ca^{2+} sensitivity of DUOX1 H_2O_2 synthesis depends on NADPH. The data also showed that, in *in vivo*-like conditions, i.e. in the presence of NADPH and expected low intracellular Ca^{2+}, maximal stimulation of DUOX1 occurs at exceptionally high Ca^{2+} concentrations that could only transiently exist in micro or nanodomains near Ca^{2+} release sites that others have documented [22]. This observation is consistent with reported association of DUOX1 and IP3R1 in T-cells [24]. Finally, preincubation of DUOX1 in Ca^{2+} concentrations normally found after stimulation of cells followed by exposure to NADPH resulted in a biphasic progress curve. A full understanding of nonlinear DUOX1 progress curves will require studies with purified and fully active enzyme. Since highly purified DUOX1 is reported to lose most activity [5], modification of the purification procedure or assay conditions will be required to explore these mechanisms.

Previous work from this lab shows that purinergic or ionophore stimulation of epithelia led to rapid increases in DUOX1 activity that returned toward baseline even with continued Ca^{2+} elevations in the case of ionophore [3]. Those studies did not have sufficient time resolution to quantify the maximum H_2O_2 synthesis rate and were not designed to give subcellular resolution of the induced Ca^{2+} transient. The studies presented here allow speculation that this maximal Ca^{2+}-stimulated DUOX1 activity may occur in a short-lived, very high [Ca^{2+}] microdomain adjacent to DUOX1 and the return toward baseline in continued elevated Ca^{2+} reflects DUOX1's lower activity in the range of Ca^{2+} concentrations (0.1 – 1 μM) typically thought sufficient to stimulate of Ca^{2+} sensitive activities. Thus, the data are consistent with the previously reported DUOX1 association to Ca^{2+} release channels being functionally important.

The dependence of DUOX1 Ca^{2+} sensitivity on NADPH might provide a mechanism to make DUOX1 more responsive when cellular [NADPH] is low and moderate its response when [NADPH] is high, thus perhaps limiting DUOX1 H_2O_2 synthesis to a narrower range of activity and limiting spatial distribution of the synthesized H_2O_2.

Funding

This work was supported by the Department of Cell Biology Faculty Incentive Fund.

CRediT authorship contribution statement

Gregory E. Conner: Writing – original draft, Visualization, Methodology, Investigation, Formal analysis, Data curation, Conceptualization.

Declaration of competing interest

The authors declare that they have no known competing financial interests or personal relationships that could have appeared to influence the work reported in this paper.

Data availability

Data will be made available on request.

Acknowledgment

I thank Drs. Peter Larsson and Arun Malhotra for valuable comments and discussions.

Appendix A. Supplementary data

Supplementary data to this article can be found online at https://doi.org/10.1016/j.redox.2024.103251.

References

[1] H. Sies, Hydrogen peroxide as a central redox signaling molecule in physiological oxidative stress: oxidative eustress, Redox Biol. 11 (2017) 613–619. PubMed PMID: 28110218.

[2] S. Morand, T. Ueyama, S. Tsujibe, N. Saito, A. Korzeniowska, T.L. Leto, Duox maturation factors form cell surface complexes with Duox affecting the specificity of reactive oxygen species generation, Faseb. J. 23 (4) (2009) 1205–1218. PubMed PMID: 19074510.

[3] G.E. Conner, Regulation of dual oxidase hydrogen peroxide synthesis results in an epithelial respiratory burst, Redox Biol. 41 (2021) 101931. PubMed PMID: 33743241.

[4] S. Rigutto, C. Hoste, H. Grasberger, M. Milenkovic, D. Communi, J.E. Dumont, B. Corvilain, F. Miot, X. De Deken, Activation of dual oxidases Duox1 and Duox2: differential regulation mediated by camp-dependent protein kinase and protein kinase C-dependent phosphorylation, J. Biol. Chem. 284 (11) (2009) 6725–6734. PubMed PMID: 19144650.

[5] J.X. Wu, R. Liu, K. Song, L. Chen, Structures of human dual oxidase 1 complex in low-calcium and high-calcium states, Nat. Commun. 12 (1) (2021) 155. PubMed PMID: 33420071.

[6] J. Sun, Structures of mouse DUOX1-DUOXA1 provide mechanistic insights into enzyme activation and regulation, Nat. Struct. Mol. Biol. 27 (11) (2020) 1086–1093. PubMed PMID: 32929281.

[7] M.V. Gattas, A. Jaffe, J. Barahona, G.E. Conner, Proton channel blockers inhibit Duox activity independent of Hv1 effects, Redox Biol. 28 (2020) 101346. PubMed PMID: 31678720.

[8] F. Barigelletti, Effect of temperature on the photophysics of rhodamine 101 in a polar solvent, Chem. Phys. Lett. 140 (6) (1987) 603–606.

[9] J.N. Barrett, S. Rincon, J. Singh, C. Matthewman, J. Pasos, E.F. Barrett, S. M. Rajguru, Pulsed infrared releases Ca(2+) from the endoplasmic reticulum of cultured spiral ganglion neurons, J. Neurophysiol. 120 (2) (2018) 509–524. PubMed PMID: 29668377.

[10] W.M. Nauseef, Detection of superoxide anion and hydrogen peroxide production by cellular NADPH oxidases, Biochim. Biophys. Acta 1840 (2) (2014) 757–767. PubMed PMID: 23660153.

[11] B. Zhao, F.A. Summers, R.P. Mason, Photooxidation of Amplex Red to resorufin: implications of exposing the Amplex Red assay to light, Free Radic. Biol. Med. 53 (5) (2012) 1080–1087. PubMed PMID: 22765927.

[12] V. Mishin, D.E. Heck, D.L. Laskin, J.D. Laskin, The amplex red/horseradish peroxidase assay requires superoxide dismutase to measure hydrogen peroxide in the presence of NAD(P)H, Free Radic. Res. 54 (8–9) (2020) 620–628. PubMed PMID: 32912004.

[13] T.V. Votyakova, I.J. Reynolds, Detection of hydrogen peroxide with Amplex Red: interference by NADH and reduced glutathione auto-oxidation, Arch. Biochem. Biophys. 431 (1) (2004) 138–144. PubMed PMID: 15464736.

[14] D.M. Bers, C.W. Patton, R. Nuccitelli, A practical guide to the preparation of Ca(2+) buffers, Methods Cell Biol. 99 (2010) 1–26. PubMed PMID: 21035681.

[15] D. Deme, A. Virion, N.A. Hammou, J. Pommier, NADPH-dependent generation of H2O2 in a thyroid particulate fraction requires Ca2+, FEBS Lett. 186 (1) (1985) 107–110. PubMed PMID: 3924659.

[16] F. Augsburger, D. Rasti, Y. Cambet, V. Jaquet, NOX5 cell-free assay for the high-throughput screening of small molecules, Methods Mol. Biol. 1982 (2019) 103–111. PubMed PMID: 31172468.

[17] C.M. Ribeiro, A.M. Paradiso, U. Schwab, J. Perez-Vilar, L. Jones, W. O'Neal, R. C. Boucher, Chronic airway infection/inflammation induces a Ca2+i-dependent hyperinflammatory response in human cystic fibrosis airway epithelia, J. Biol. Chem. 280 (18) (2005) 17798–17806. PubMed PMID: 15746099.

[18] G.E. Glock, P. McLean, The intracellular distribution of pyridine nucleotides in rat liver, Exp. Cell Res. 11 (1) (1956) 234–236. PubMed PMID: 13356851.

[19] Y. Ogasawara, M. Funakoshi, K. Ishii, Determination of reduced nicotinamide adenine dinucleotide phosphate concentration using high-performance liquid chromatography with fluorescence detection: ratio of the reduced form as a biomarker of oxidative stress, Biol. Pharm. Bull. 32 (11) (2009) 1819–1823. PubMed PMID: 19881290.

[20] R.P. Goodman, S.E. Calvo, V.K. Mootha, Spatiotemporal compartmentalization of hepatic NADH and NADPH metabolism, J. Biol. Chem. 293 (20) (2018) 7508–7516. PubMed PMID: 29514978.

[21] R. Tao, Y. Zhao, H. Chu, A. Wang, J. Zhu, X. Chen, Y. Zou, M. Shi, R. Liu, N. Su, J. Du, H.M. Zhou, L. Zhu, X. Qian, H. Liu, J. Loscalzo, Y. Yang, Genetically encoded fluorescent sensors reveal dynamic regulation of NADPH metabolism, Nat. Methods 14 (7) (2017) 720–728. PubMed PMID: 28581494.

[22] M.R. Tadross, R.W. Tsien, D.T. Yue, Ca2+ channel nanodomains boost local Ca2+ amplitude, Proc Natl Acad Sci U S A 110 (39) (2013) 15794–15799. PubMed PMID: 24019485.

[23] D. Gil, A.H. Guse, G. Dupont, Three-dimensional model of sub-plasmalemmal Ca(2+) microdomains evoked by the interplay between ORAI1 and InsP(3) receptors, Front. Immunol. 12 (2021) 659790. PubMed PMID: 33995380.

[24] J. Kwon, K.E. Shatynski, H. Chen, S. Morand, X. de Deken, F. Miot, T.L. Leto, M. S. Williams, The nonphagocytic NADPH oxidase Duox1 mediates a positive feedback loop during T cell receptor signaling, Sci. Signal. 3 (133) (2010) ra59. PubMed PMID: 20682913.

[25] O. Dellis, S.G. Dedos, S.C. Tovey, R. Taufiq Ur, S.J. Dubel, C.W. Taylor, Ca2+ entry through plasma membrane IP3 receptors, Science 313 (5784) (2006) 229–233. PubMed PMID: 16840702.

[26] B. Honore, H. Vorum, The CREC family, a novel family of multiple EF-hand, low-affinity Ca(2+)-binding proteins localised to the secretory pathway of mammalian cells, FEBS Lett. 466 (1) (2000) 11–18. PubMed PMID: 10648803.

[27] Q.T. Lin, R. Lee, A.L. Feng, M.S. Kim, P.B. Stathopulos, The leucine zipper EF-hand containing transmembrane protein-1 EF-hand is a tripartite calcium, temperature, and pH sensor, Protein Sci. 30 (4) (2021) 855–872. PubMed PMID: 33576522.

[28] A. Yang, S. Miron, P. Duchambon, L. Assairi, Y. Blouquit, C.T. Craescu, The N-terminal domain of human centrin 2 has a closed structure, binds calcium with a very low affinity, and plays a role in the protein self-assembly, Biochemistry 45 (3) (2006) 880–889. PubMed PMID: 16411764.

[29] J.F. Morrison, The slow-binding and slow, tight-binding inhibition of enzyme-catalyzed reactions, Trends Biochem. Sci. 7 (3) (1982) 102–105. PubMed PMID: WOS:A1982NG18400014.

[30] G.R. Ainslie Jr., J.P. Shill, K.E. Neet, Transients and cooperativity. A slow transition model for relating transients and cooperative kinetics of enzymes, J. Biol. Chem. 247 (21) (1972) 7088–7096. PubMed PMID: 4343169.

[31] S.G. Waley, The kinetics of substrate-induced inactivation, Biochem. J. 279 (Pt 1) (1991) 87–94. PubMed PMID: 1930157.

[32] C. Dupuy, D. Deme, J. Kaniewski, J. Pommier, A. Virion, Ca2+ regulation of thyroid NADPH-dependent H2O2 generation, FEBS Lett. 233 (1) (1988) 74–78. PubMed PMID: 3133245.

[33] T. Sasaki, T. Kikuchi, N. Yumoto, N. Yoshimura, T. Murachi, Comparative specificity and kinetic studies on porcine calpain I and calpain II with naturally occurring peptides and synthetic fluorogenic substrates, J. Biol. Chem. 259 (20) (1984) 12489–12494. PubMed PMID: 6092335.

[34] Z.X. Liu, K. Yu, J. Dong, L. Zhao, Z. Liu, Q. Zhang, S. Li, Y. Du, H. Cheng, Precise prediction of calpain cleavage sites and their aberrance caused by mutations in cancer, Front. Genet. 10 (2019) 715. PubMed PMID: 31440276.

[35] A. Baici, Slow-onset enzyme inhibition and inactivation, in: C. Kettner, M.G. Hicks (Eds.), Experimental Standard Conditions of Enzyme Characterizations – Protein Structure Meets Enzyme Kinetics Proceedings of the International Beilstein Symposium on Experimental Standard Conditions of Enzyme Characterizations, Logos Verlag Berlin, Berlin, 2012, pp. 55–73.